ADVANCED ENERGY MATERIALS
www.advenergymat.de

The Value of Device Characterization for the Optimization of Organic Solar Cells

Leonard Christen, Barbara Urbano, Anne Krause, Paula Hartnagel, and Thomas Kirchartz**

In addition to achieving record efficiencies of ≈20%, organic photovoltaics (OPV) has to overcome several additional challenges. These include researching environmentally friendly solvents, improving stability, yield, and scaling up to industrial standards in terms of cell size and mass production. However, identifying the optimal candidates from the countless material combinations and determining the exact process parameters is like looking for a needle in a haystack. Process optimization usually comprises phases such as device fabrication, measurement, and evaluation, concluding with the experimental design of the next round of device making. Given the extent of the process parameter space, this optimization process can be extremely time-consuming. However, as optimization algorithms mainly based on mathematical models become more prevalent in automated laboratories, the question arises of how to include physics domain knowledge based on device characterization of the samples into the algorithmic optimization process. To address this question, a benchmark function is created using experimental solar cell data originating from hundreds of organic solar cells prepared with different processing conditions. This benchmark function is used to test and compare different optimization approaches to quantify under which conditions physical domain knowledge can improve the speed of process optimization in an experimental laboratory.

1. Introduction

Owing to modern machine-learning algorithms and increasingly automated laboratories, the optimization of processes to fabricate materials and devices with a well-defined functionality has experienced considerable acceleration in recent years.[1–6] Standard approaches in the field of process optimization based on machine learning typically rely on mathematical models that attempt to establish a direct correlation between the process parameters and figures of merit, which, in the case of solar cells, could be photovoltaic efficiencies potentially combined with metrics of cost and stability.[7,8] The question arises as to whether characterization methods that aim to establish a better quantitative understanding of the link between the material and device parameters can provide additional benefits for process optimization. The current reality in many laboratories working on solution-processable photovoltaics or optoelectronics is based on a few simple measurements used for process optimization combined with more sophisticated a posteriori experiments to explain the benefits and features of the optimized process. The question of how far further knowledge about material parameters is fundamentally useful to accelerate process optimization or only useful to satisfy human curiosity becomes exceedingly important the more the process of technology optimization becomes algorithmic, i.e., following the mathematical logic of an optimization algorithm – however complicated it may be.

To address this question, we have implemented a virtual laboratory using a large amount of current-voltage (*JV*) curves of organic solar cells prepared with different processing conditions. This virtual laboratory serves as a benchmark function to model the entire optimization process that is, from the cell manufacturing process to characterization and evaluation. This benchmark function can then be used to compare different optimization approaches that contain different degrees of knowledge and understanding of material properties and solar cell device physics. This could not easily be done with reasonable statistics by comparing optimization processes in the laboratory but requires the detour via the virtual laboratory. By comparing different optimization approaches using our experimentally backed benchmark function, we want to answer the implicit question posed by the title. We want to understand how valuable device characterization

L. Christen, B. Urbano, A. Krause, P. Hartnagel, T. Kirchartz
IMD3-Photovoltaik
Forschungszentrum Jülich
52425 Jülich, Germany
E-mail: l.christen@fz-juelich.de; t.kirchartz@fz-juelich.de

T. Kirchartz
Faculty of Engineering and CENIDE
University of Duisburg-Essen
Carl-Benz-Str. 199, 47057 Duisburg, Germany

The ORCID identification number(s) for the author(s) of this article can be found under https://doi.org/10.1002/aenm.202500247

DOI: 10.1002/aenm.202500247

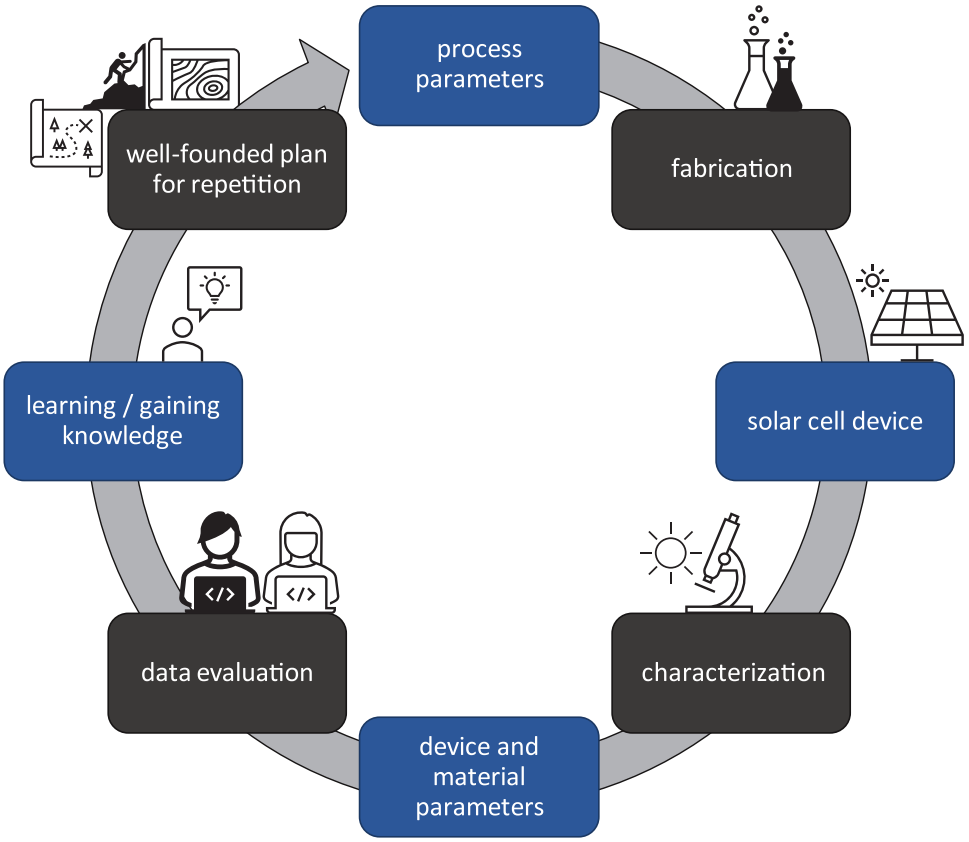

Figure 1. Standard experimental process optimization loop. The loop starts with the selection of process parameters. The solar cell is manufactured in the laboratory (or factory) and then characterized. How the device information is to be used determines which characterization methods are necessary. A pure black-box optimization only requires the measurement of the figure of merit used for optimization, such as solar cell efficiency. Modern optimization algorithms then use this information efficiently to suggest new process parameters. Creating a solid understanding usually requires measurements beyond those principal figures of merit and access to material parameters such as charge-carrier mobilities or recombination coefficients. In contrast to black-box optimization, the newly generated knowledge extends the experience and intuition of the researcher, based on which new process parameters can be selected. Regardless of the optimization approach, the next step is to gain knowledge from the measured data to plan a repetition of the entire cycle.

is for the purpose of optimizing a given process for maximum efficiency.

In recent years, tremendous progress has been made in the field of organic photovoltaics (OPV), especially after non-fullerene acceptors have entered the scene. Thus, record efficiencies of ≈20% at one sun intensity and > 30% for indoor lighting conditions have been reported.[9–17] In addition to high efficiencies also high device stability and the possibility of upscaling processes to larger areas using high-yield roll-to-roll processes in air with non-halogenated solvents are important requirements for industrialization.[18–23]

Thus, more research is needed to make OPV competitive with conventional silicon-based solar applications. An immense number of different material combinations with various processing approaches is conceivable.[24–26] Therefore, the ability to efficiently investigate the resulting high-dimensional parameter space to find the optimal parameter combination is a fundamental requirement. In certain situations, constrained optimization might be required; for instance, if the condition of high-yield fabrication (low percentage of non-working devices) in a non-clean room environment implies that the active layer thickness should not be lower than a certain threshold thickness. In these situations, efficiencies need to be optimized, subject to an additional condition related to the active layer thickness.[27–29]

Figure 1 shows a schematic representation of a general process optimization loop in the field of photovoltaics that can be easily generalized to other functional devices. The starting point is a set of process parameters with which the first set of solar cells is fabricated. The cells are then characterized, to better understand the efficiency-limiting material and interface properties. The resulting knowledge is subsequently used to decide with which process conditions the cycle should be repeated.

The classic approach would be to use various characterization methods to understand the fundamental physical relationships between process, device, and material parameters, as well as the actual figure of merit (efficiency, stability, etc...). Scientists gain increasing experience over time and may even develop some intuition based on which process optimization is performed, for example, some relationships could be transferred to other material systems. In increasingly complex and high-dimensional parameter spaces, with sometimes strongly (non-linearly) correlating or

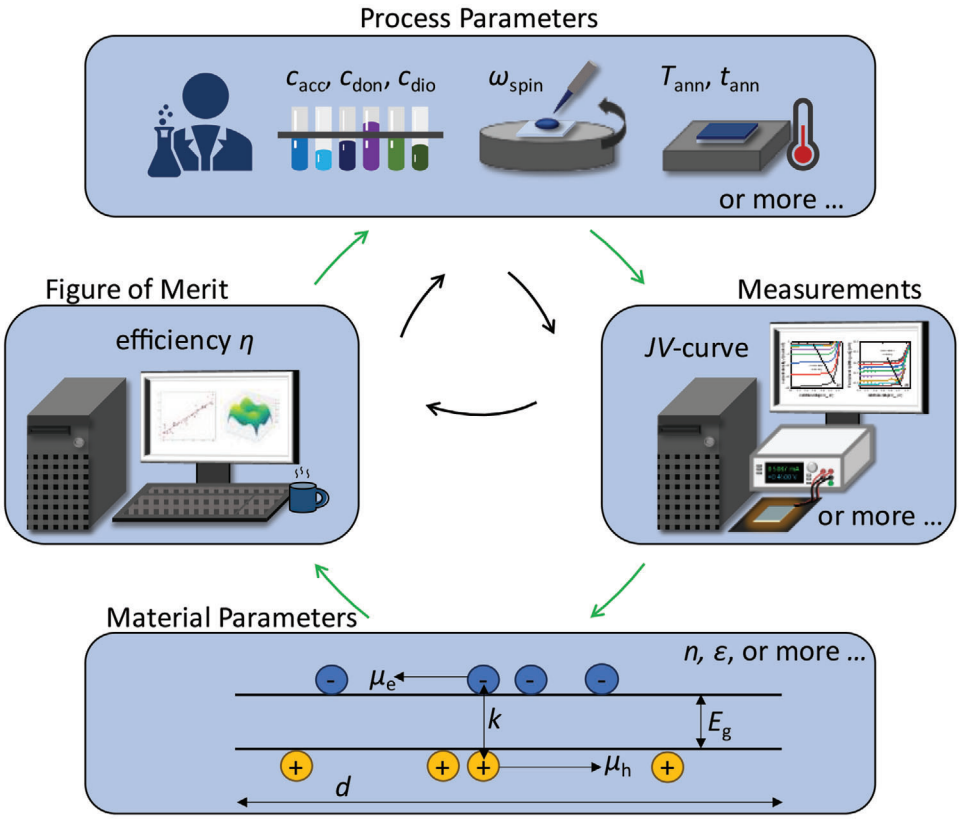

Figure 2. Black-box (black circle) and model-based optimization processes (green circle) are compared in this study. Instead of investigating the correlations between process parameters such as chemical concentrations, spin speed, or annealing conditions and the figure of merit, here the efficiency η, we search for the correlations between process parameters and device as well as material parameters such as charge-carrier mobility and lifetimes or the active layer thickness to calculate the efficiency from these parameters. The use of additional information about the physical background, such as interference within the layer system, can speed up the optimization process.

even unknown influences, increasingly complex models are required, and human intuition will reach its limit.

As already mentioned, modern process optimization methods such as Bayesian optimization rely on mathematical-statistical approaches, whereas physical relationships often play no, or only a subordinate role in process optimization.[30–32] An advantage of these methods is the manageability of large datasets in multidimensional parameter spaces as well as the option to create self-driven laboratories or a fully automated workflow.[33–36] However, the algorithm used only "learns" the correlation between input variables (process parameters) and output variables (figures of merit) during the repetitive cycles. The optimization algorithm does not "know" or is trained with the basics of optics or physics of semiconducting devices that a human expert would be aware of. So far, a couple of promising approaches for improving Bayesian optimization with the help of expert knowledge have been published in slightly different contexts.[37–39] The term "gray-box" is also used in this context and originates from the idea of combining a black-box with a so-called white-box, which is entirely based on physical models.[40] The extent to which expert knowledge is used can vary. From prior-guided optimization to the use of complex (physical) models. The latter is also known as composite objective Bayesian optimization.[41,42]

In this paper, we show for the test case of OPV that the inclusion of additional measurement data can potentially accelerate existing process optimization methods. We will see that the degree of acceleration of process optimization by physics domain knowledge depends dramatically on the complexity of the optimization problem.

The basic idea of our comparison between different optimization approaches is illustrated in **Figure 2**. Instead of looking for correlations between process parameters and efficiency, we find correlations between process parameters and device- and material parameters to calculate the efficiency from these parameters. In this way, it is possible to combine the advantages of expert-based optimization and machine learning-based optimization, i.e., a combination of a specialist's domain knowledge, as well as the ability to handle large multidimensional data.

2. A Virtual Laboratory as Benchmark Function

Optimization approaches are often tested using different multidimensional, analytical benchmark functions.[43–45] In general, benchmark functions have the great advantage that they are well known. Therefore, different optimization algorithms can not only be compared relatively with each other but also be evaluated in absolute terms. Additionally, a benchmark function can

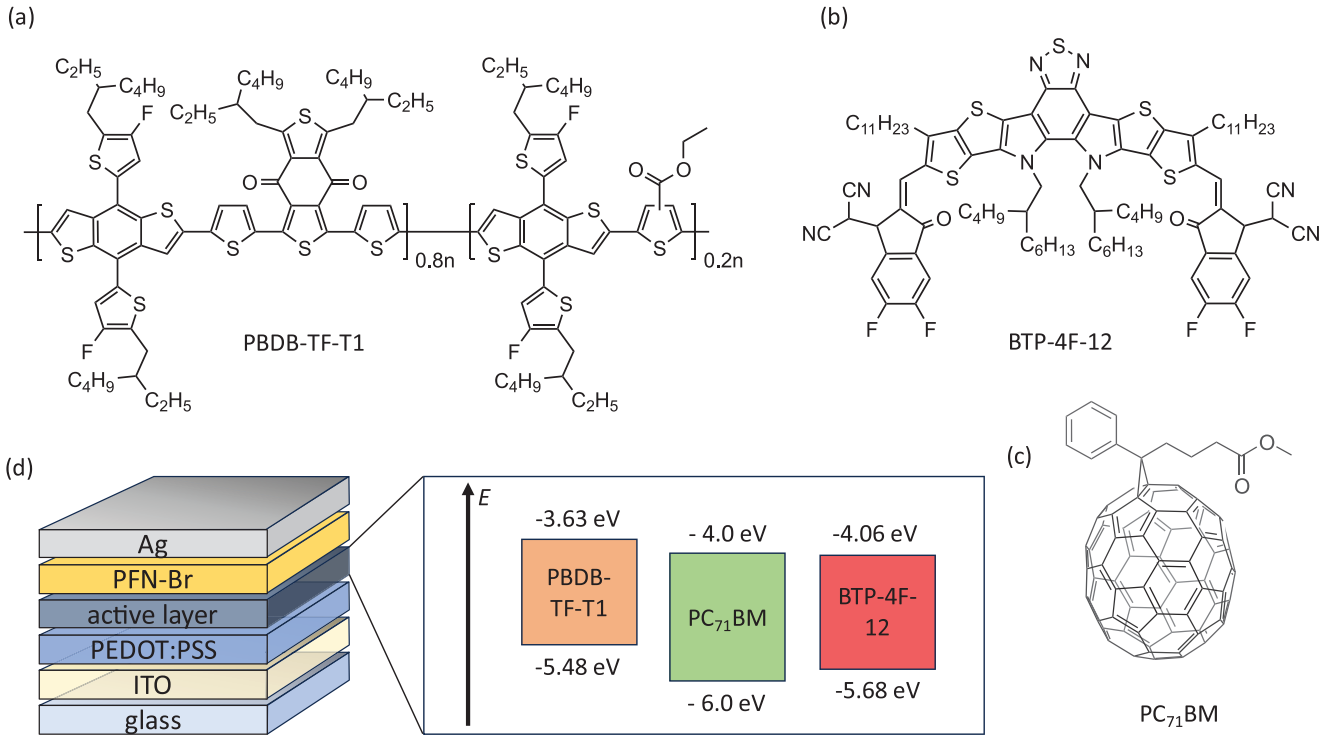

Figure 3. Molecular structures and layer stack of the fabricated solar cells: a) PBDB-TF-T1 (donor), b) BTP-4F-12 (acceptor-1), and c) $PC_{71}BM$ (acceptor-2). d) The layer stack for the solar cells is glass / ITO / PEDOT:PSS / active layer / PFN-Br / Ag with energy levels for the active layer.[46,47].

usually be sampled extremely quickly, which enables extensive statistical analysis.

However, these benchmark functions could not be used to solve the problem at hand. First, with analytical benchmark functions, we could not ensure to have a similar complexity to a real-life optimization problem in OPV. Second, we could not perform model-based optimization on an analytical benchmark function that is incompatible with the physical model in question. Thus, the only feasible approach is to create enough experimental data to create a sufficiently good benchmark function that captures the physics and chemistry of the specific problem of organic solar cell optimization.

This benchmark function cannot to be used to optimize a specific solar cell process. Instead, the solar cell process must be already optimized at this stage and all data on the path towards optimization are now included to build up the benchmark function. This function is then used to investigate (in the form of mathematical thought experiments) what the best approach would be to optimize the efficiency versus process parameter landscape that is defined by (essentially) a multidimensional interpolation of the experimental data. In contrast to the standard analytical benchmark functions, which are deliberately generic, the findings based on this virtual laboratory are transferable to typical optimization problems in the field of OPV.

The starting points for our virtual laboratory are a few hundred solar cells manufactured using different process parameters, as well as measured *JV* curves and active layer thicknesses measured non-destructively using capacitance measurements at reverse bias. The layer stack is glass / ITO / PEDOT:PSS / active layer / PFN-Br / Ag, where the active layer is a ternary mixture of PBDB-TF-T1:BTP-4F-12:$PC_{71}BM$. **Figure 3**a–c shows the used molecules and

Figure 3d shows the layer stack for the solar cell with the energy levels for the active layer from literature measured via cyclic voltammetry.[46,47] The 6 process parameters are the ratio of donor to acceptor material ($c_{\text{PBDB-TF-T1}}/c_{\text{Acc}}$), the proportion of both acceptors ($c_{\text{BTP-4F-12}}/c_{\text{Acc}}$), the amount of 1,8-diiodooctane (c_{DIO}), the spin speed during the coating of the active layer (ω_{spin}), as well as bakeout temperature (T_{ann}) and time (t_{ann}). More detailed information is provided in the Supporting Information. One vector of process parameters is called $\mathbf{\Theta}_{\mathbf{pro}}$.

To keep the device model simple for this test case, only a few related device and material parameters were estimated: the electron and hole mobility μ, the recombination coefficient for direct electron-hole recombination k, the active layer thickness d, and the efficiency $\eta_{\text{eh}} = G_{\text{eh}}/G_{\text{opt}}$ of generating separated electron-hole pairs from excitons at a given optical generation rate G_{opt}. We assume a small influence of the process parameters on the refractive index n and the extinction coefficient k.[48] The material parameter η_{eh} can compensate for any inaccuracies in the optical model. For more information regarding the optical data, we refer to the Supporting Information. One set of material parameters is called $\mathbf{\Theta}_{\mathbf{mat}}$.

To estimate the material parameters from measured *JV* curves, we proceeded as follows: First, we used a simulation tool called Advanced Semiconductor Analysis (ASA), which can solve the Poisson equation as well as the continuity equations to simulate *JV* curves for different material parameters.[49] ASA thereby solves the forward problem of simulating *JV* curves given a set of known or assumed material parameters. The result is a database

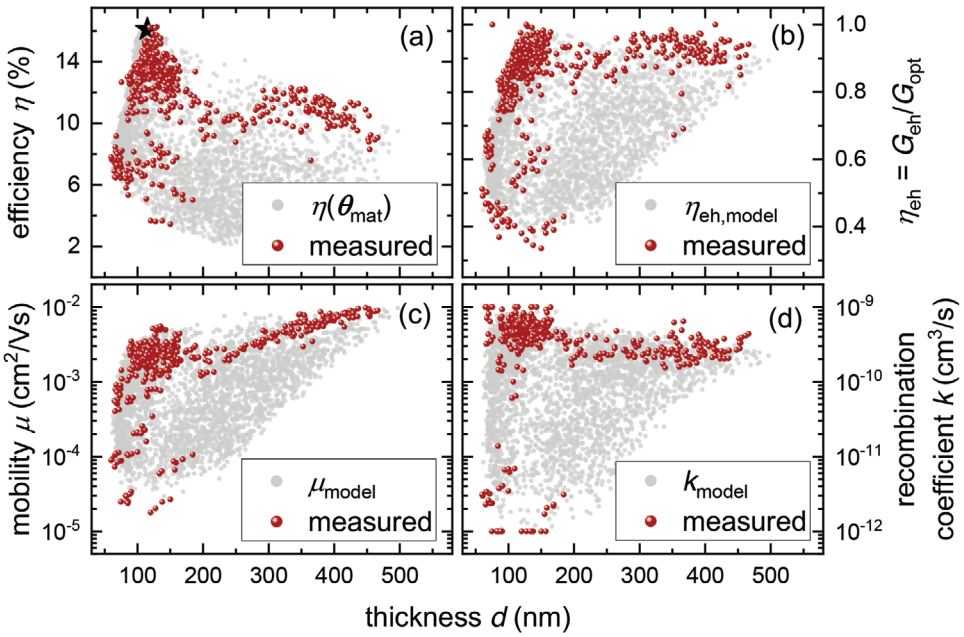

Figure 4. Comparison of the measured data and the virtual laboratory. a) The efficiencies as a function of the active layer thickness. For all measured cells shown in red the efficiency is directly calculated from the *JV* curves. The data sampled from the virtual laboratory is shown in gray and the star indicates the global optimum for the entire parameter space. b) The efficiency $\eta_{eh} = G_{eh}/G_{opt}$ of generating separated electron-hole pairs from excitons at a given optical generation rate G_{opt} as a function of the active layer thickness. c) The electron and hole mobility μ as a function of the active layer thickness. d) The recombination coefficient for direct electron-hole recombination k as a function of the active layer thickness. The material parameters shown in b) to d) are estimated from *JV* curves as described, and the thickness is measured directly. The values for the material parameters determined in this way are then used to train an SVR approximation function for each parameter in $\mathbf{\Theta}_{mat}$. All graphs are plotted as a function of the active layer thickness, although d is part of $\mathbf{\Theta}_{mat}$ as well. It can be understood as a projection of all six process parameters onto one material parameter. All modeled data points are sampled in a way to represent the entire parameter space.

with a couple of thousand sets of material parameters and associated *JV* curves. With this database, we trained a convolutional neural network to calculate a *JV* curve from a given $\mathbf{\Theta}_{mat}$ much faster.[50,51] Comparable approaches are reported by Brandt et al. and Hußner et al.[52,53] Then, using the neural network, we solve the inverse problem, namely, to find the most likely material parameters given a certain *JV* curve (or set of *JV* curves). By searching for the best-fitting simulated *JV* curve, we estimate the material parameters $\mathbf{\Theta}_{mat}$ from a measured *JV* curve fabricated using a specific set of process parameters, $\mathbf{\Theta}_{pro}$. Further details regarding ASA and the neural network are provided in the Supporting Information.

Based on the link we have now established between $\mathbf{\Theta}_{pro}$ and $\mathbf{\Theta}_{mat}$, we used support vector regression (SVR) from the Python package scikit-learn to train different models, describing the correlation between the two vectors $\mathbf{\Theta}_{mat}(\mathbf{\Theta}_{pro})$ for the entire parameter space. The SVR is used as a multidimensional function approximator. In this case, it approximates the material-parameter functions, namely $d(\mathbf{\Theta}_{pro})$, $\eta_{eh}(\mathbf{\Theta}_{pro})$, $\mu(\mathbf{\Theta}_{pro})$ and $k(\mathbf{\Theta}_{pro})$, each as a function of the 6-D process parameter space. Further information can be found in the Supporting Information.

Figure 4 shows results for the measured data as well as the resulting model prediction plotted as a function of the active layer thickness. The efficiencies calculated from the measured *JV* curves $\eta_{meas}(\mathbf{\Theta}_{pro})$ as well as the final model $\eta(\mathbf{\Theta}_{mat}(\mathbf{\Theta}_{pro}))$ both as a function of the thickness of the active layer are shown in Figure 4a. It should be noted that for measured data, the active layer thickness is also measured data, while for estimated data, the thickness itself is part of the estimated $\mathbf{\Theta}_{mat}$ and therefore a function of $\mathbf{\Theta}_{pro}$. Since the 6-D vector, $\mathbf{\Theta}_{pro}$ is difficult to visualize and for the sake of comparability in terms of measured and modeled data, we have decided to display the other material parameters also as a function of the layer thickness.

As described above, for every material/device parameter (d, η_{eh}, μ, and k) the measured data now serves as training data to find a surrogate model based on an SVR to link process parameter combinations to every one of the four chosen material/device parameters: The plots $\eta_{eh}(\mathbf{\Theta}_{pro})$, $\mu(\mathbf{\Theta}_{pro})$ and $k(\mathbf{\Theta}_{pro})$ are shown in Figure 4b–d. The gray data points in Figure 4 are discrete points that are sampled from the continuous function approximation created by the SVR. The discrete points are sampled from the SVR model using a combination of a genetic optimization algorithm and Latin hypercube sampling. This is done in a way that most of the parameter space is represented. As most of the parameter space consists of thin layers, the parameter space for low spin speed was explicitly sampled additionally. For further information as well as comparable figures for J_{SC}, V_{OC}, and the fill factor FF, we refer to the Supporting Information.

To emphasize the advantages of a benchmark function, we note that the virtual laboratory was sampled several thousand times to create Figure 4 alone. Keeping in mind, that using the presented model to link a specific $\mathbf{\Theta}_{pro}$ to $\mathbf{\Theta}_{mat}$, namely sampling from the virtual laboratory, can be understood as (virtually)

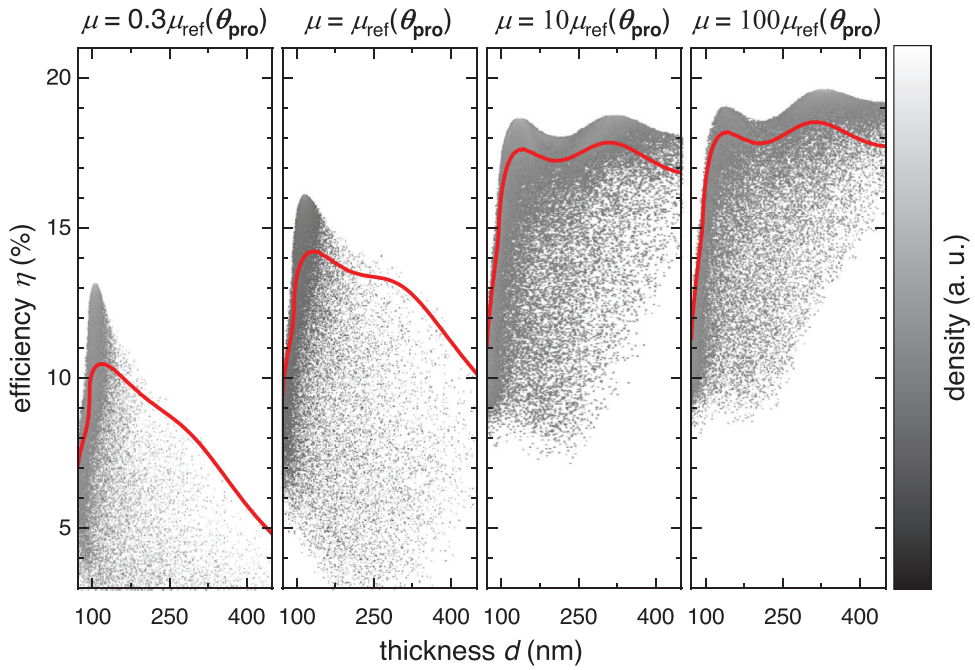

Figure 5. The efficiency as a function of $\mathbf{\Theta}_{pro}$ as a projection on the active layer thickness d for artificially decreased and increased charge-carrier mobilities. The gray areas are evaluated by a combination of a genetic optimization algorithm and Latin hypercube sampling. As most of the parameter space consists of thin layers, the parameter space for low spin speed was explicitly sampled additionally. The red line shows an example of the change in the same trajectory through the different parameter spaces with different charge-carrier mobilities. The artificial adaptation of the benchmark function is for theoretical issues, such as the development of future materials with higher charge-carrier mobility by increasing μ. It becomes clear that for higher charge-carrier mobilities a second optimum appears at higher layer thicknesses, which with higher μ also exceeds the first optimum at thin layer thicknesses.

fabricating a solar cell under well-defined process parameters, it would therefore be necessary to fabricate several thousand samples just for the figure shown.

The simulation of the JV curve corresponding to the resulting $\mathbf{\Theta}_{mat}$ by solving Poisson- and continuity equations is then analogously comparable to a (virtual) JV curve measurement. The last step, the evaluation of the (virtual) measurement to calculate the efficiency (or as well as V_{OC}, $J_{SC,}$ and fill factor) from the (virtually measured) JV curve, is no different from the work in a non-virtual laboratory.

With this virtual laboratory, the entire optimization process from Figure 2 can now be benchmarked: As in a real laboratory, the selected process parameters determine the properties of the solar cell, which are defined by the device and material parameters. However, instead of investing hours to fabricate, characterize, and evaluate a real solar cell, the loop shown in Figure 1 can be done in a few minutes when using the virtual laboratory. As already mentioned, the virtual laboratory is only intended to serve as an improved benchmark function. Thus, the key requirement for the quality and number of experimental data points is not as high as to have predictive power over the whole parameter space of this one blend but only to have enough data to create this benchmark function with a realistic level of complexity that is representative for a typical organic solar cell optimization scenario daily experienced by many labs around the world. Further insights into the virtual laboratory such as 2D sectional planes through the hypersurface, which are more tangible for humans, can be found in the Supporting Information.

Another advantage of this virtual laboratory is the fact that we can change the entire parameter space in a well-defined way. For answering the question of how useful device characterization is, it is very important how complex the parameter space is. The more the parameter space resembles just one multidimensional global optimum with few additional features, the easier it is for any algorithm to find the optimum. The more complex and feature-rich the parameter space is, the more physics-domain knowledge might help. One way of testing this hypothesis is to increase the mobility within our virtual laboratory until the second interference maximum becomes the global efficiency optimum to test how that affects the balance between black-box and model-based optimization.

How the parameter space changes as a function of mobility can be seen exemplarily in **Figure 5**, which shows the efficiencies of the multidimensional space projected for simplicity onto 1D, in this case, the thickness. The reference mobility μ_{ref} is the mobility, which results from the analysis of the experimental data. The prefactor for μ varies from 0.3 up to 100.

3. Process Optimization

In principle, various optimization strategies can be considered for the model-based optimization approach. The decisive factor is that the optimization algorithm is based on approximating the true function with a surrogate model, which can then benefit from domain knowledge. Bayesian optimization is becoming increasingly popular in materials science as well as in OPV.[6,34,54,55]

The main reason Bayesian optimization fits well for the work in an actual laboratory is that this algorithm is designed to find the global optimum of (high dimensional) processes that are expensive to evaluate and that it offers useful solutions for noisy parameter spaces.[32] Therefore, we used this optimization strategy as a test case to compare black-box and model-based process optimization.

We start the process optimization with 18 (virtually) fabricated solar cells selected via a Latin hypercube sampling in an initial first round. To ensure a reliable optimization and to prevent the starting condition from influencing the comparability of the approaches mentioned above, the entire optimization procedure was repeated with different starting conditions multiple times.[56] Therefore, a total of 50 different starting conditions were defined, which then remained the same for all optimization runs. For more details regarding the optimization algorithm (and also on the stability of the used algorithm), we refer to the Supporting Information.

For each further optimization iteration, two proposals are given. One proposal is for exploration, and one is for exploitation. In detail, we train a Gaussian process regressor (GPR) also using the Python package scikit-learn to model a regression function with an associated standard deviation. The proposal selection of the new data points is then based on the most likely estimated value (exploitation) as well as the uncertainty (exploration).

From this point on, a distinction must be made between the different optimization approaches. In detail, the following optimization approaches are compared to answer the initial question of the extent to which measurements that go beyond determining efficiency only can improve the optimization process, as well as to search for process optimization improvements in finding high active layer thickness solar cells:

- $\eta_{\mathrm{BB}}(\mathbf{\Theta}_{\mathbf{pro}})$: The regression function predicting the efficiency from process parameters is based on the calculated correlation exactly between these two types of data, the figure of merit η and the process parameters $\mathbf{\Theta}_{\mathbf{pro}}$. This approach does not "know" or "learn" anything about the underlying physics and is a black-box optimization.
- $\eta_{\mathrm{BB}}(\mathbf{\Theta}_{\mathbf{pro}})$, and $d_{\mathrm{fit}}(\mathbf{\Theta}_{\mathbf{pro}})$: As in the first approach the fit function is directly based on the process parameters. To also include extended restriction options for the active layer thickness, a separate GPR is trained to describe the correlation between the thickness d and $\mathbf{\Theta}_{\mathbf{pro}}$.
- $\eta_{\mathrm{model}}(\mathbf{\Theta}_{\mathbf{mat}})$: Different from the pure black-box approach, the regression function here is not directly based on the process parameters. Instead, the material parameters in $\mathbf{\Theta}_{\mathbf{mat}}$, namely μ, k, d, and η_{eh} are correlated with $\mathbf{\Theta}_{\mathbf{pro}}$. Instead of one GPR model, the result is four GPR models, one for each material parameter. The resulting efficiency (expected value and uncertainty) then is calculated, by solving Poisson and continuity equations as described above.
- $\eta_{\mathrm{model}}(\mathbf{\Theta}_{\mathbf{mat}})$ with $d_{\mathrm{true}}(\mathbf{\Theta}_{\mathbf{pro}})$: This approach is similar to $\eta_{\mathrm{model}}(\mathbf{\Theta}_{\mathbf{pro}})$, but the active layer thickness is not estimated from a GPR model but is always assumed to be known. In terms of solar cell fabrication, this can best be understood as a fully controllable active layer thickness during the fabrication process, maybe by in situ measurements and corresponding process adjustments, i.e., during slot die coating or roll-to-roll procedures in industrial solar cell fabrication[57].

To add restrictions, such as a minimum layer thickness, different procedures are chosen for the different approaches. Because the layer thickness is not explicitly considered in the black-box approach $\eta_{\mathrm{BB}}(\mathbf{\Theta}_{\mathbf{pro}})$, a limitation is possible by directly adjusting the training data accordingly. To achieve a layer thickness constraint, the efficiency of cells with a layer thickness less than the minimum layer thickness is set to zero in this test case. In all other approaches, the fit function of the layer thickness can be modified according to the constraint. The training data is not changed here. Instead, the predicted efficiency is set to zero where the fit function of the layer thickness is smaller than the minimum layer thickness.

A major advantage of using a known benchmark function is the ability to compare the results in absolute terms with the global optimum. As mentioned above, for the comparison of the different approaches, for each optimization procedure a fixed number of iterations was selected after a random selection of identical starting points. Since the true optimum is usually unknown in the case of process optimization in an actual laboratory, it should be noted that the model-based approach using a Bayesian optimization strategy is compatible with different termination criteria commonly used in Bayesian optimization. In addition to directly limiting the number of iterations, it is also conceivable to define a termination routine based on a detectable plateau formation during process optimization, or in other words, to detect if the algorithm is converging. It should also be noted that an inherent advantage of model-based optimization is that the predicted figure of merit, e.g. the efficiency, must always be within physically reasonable limits. It is therefore less likely that the benefits of an exploratory measurement will be overestimated. For more details regarding the convergence of the used optimization algorithm, we refer to the Supporting Information. Using a different acquisition function based on the expected improvement, the probability of improvement, or the knowledge gradient is particularly effective, to improve the optimization algorithm.

4. Results

In this section, we present different findings obtained from the virtual laboratory as an improved benchmark function. We only show a small representative selection of all results. **Figure 6** illustrates the results of a randomly selected optimization run for two different parameter spaces. The first parameter space has only one global optimum; for the second parameter space, a second optimum appears at a layer thickness of 328 nm and becomes the global optimum. Figure 6a,b show that for $\mu = \mu_{\mathrm{ref}}$ there is no significant difference between the pure black-box and the model-based optimization approaches. However, for an inflated charge-carrier mobility, as shown in Figure 6c,d only the model-based optimization approach manages to find the global optimum at the high thickness within the limited number of iterations.

As already mentioned above, the results of a single optimization run can depend on the initial database, i.e., we performed a total of 50 runs per approach and parameter space and statistically analyzed the results. To do this, we selected the highest efficiency and determined the average, minimum, and maximum

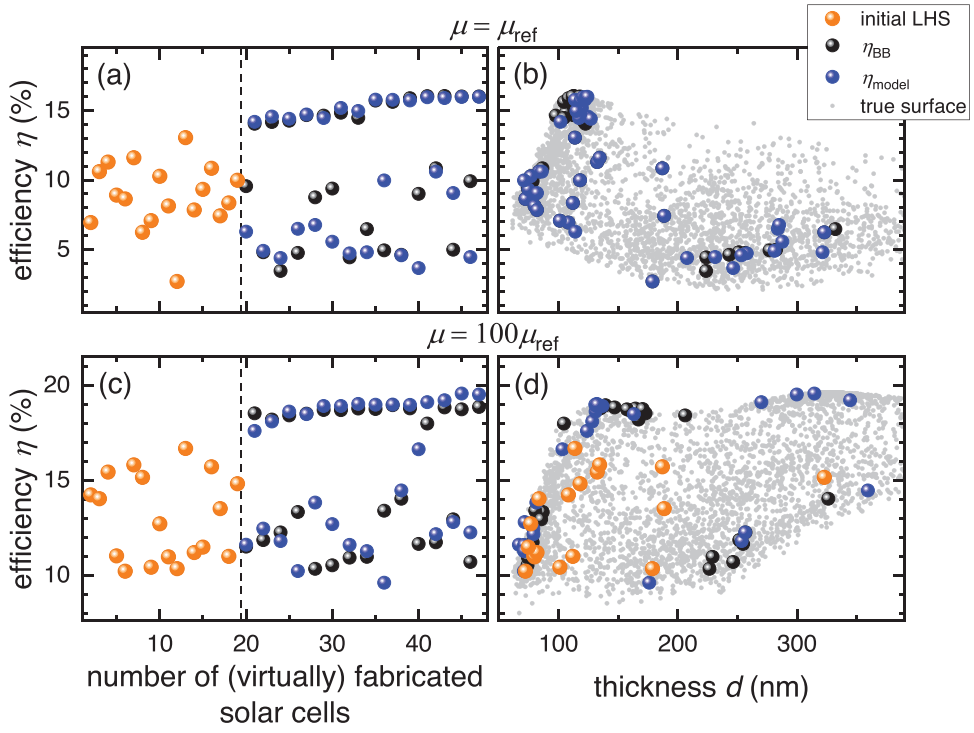

Figure 6. The two different optimization approaches for two parameter spaces, $\mu = \mu_{ref,}$ and $\mu = 100\mu_{ref}$, with no active layer thickness restriction. a) Efficiency as a function of the number of (virtually) fabricated solar cells. The dashed lines separate the initial Latin hypercube sampling (18 cells illustrated in orange) and the consecutive optimization rounds (illustrated in black for the black-box approach, and in blue for the model-based approach). The slight increase in the measurement points in the upper area of the figure is due to exploitation, the strongly distributed area at low efficiencies is due to exploration. b) The efficiency as a function of the layer thickness for the same optimization run is shown. The gray data points are sampled from the true parameter space to allow a better comparison. c,d) Analogue figures for the second parameter space with $\mu = 100\mu_{ref}$. While there is no significant difference for lower charge-carrier mobilities, for $\mu = 100\mu_{ref}$, it becomes clear that, in contrast to the black-box approach, the model-based approach finds the second optimum at higher layer thicknesses.

values as well as the distribution of the values for each round for all optimization approaches and parameter spaces. For a more in-depth understanding, we have performed the same with the layer thicknesses associated with the selected efficiencies. **Figure** 7 shows some of these results. For each optimization approach and charge-carrier mobility variation, there are 4 figures associated. One displays the mean efficiencies as a function of the optimization round, including the minimum-maximum interval, while the other shows the corresponding median layer thicknesses also with the minimum-maximum range. Adjacent to each, there is a histogram of both quantities, where the different distributions per round are cumulatively added. Thus, the histogram can be understood as the integrated distribution of the data within the minimum-maximum ranges. Figure 7a, for example, shows a continuous improvement in the efficiency for each round of pure black-box optimization and how the active layer thickness changes with each round of optimization for $\mu = \mu_{ref}$.

A comparison of Figure 7a–f shows that the additional fitting of the material parameters offers a significant advantage over the pure black-box optimization $\eta_{BB}(\mathbf{\Theta}_{pro})$ when a second optimum appears at higher thicknesses. An initial explanation for this improvement is due to the additional information about the layer thickness, it seems to cause the non-pure black-box approach to search significantly faster in the area around the correct layer thickness.

This observation can be seen even more clearly in **Figure** 8a–d. The more information is used during the different process optimization approaches, the better the results delivered by the corresponding approach. Figure 8 shows that the variation in layer thickness decreases with increasing information content during the process optimization. While the black-box approach only learns the direct correlation between η and $\mathbf{\Theta}_{pro}$, the model-based approaches can eventually predict the required target layer thickness. This "understanding" of the influence of the layer thickness on the efficiency, is particularly strong in the model-based approach with an adjustable layer thickness, namely $\eta_{model}(\mathbf{\Theta}_{mat})$ with d_{true}.

Looking at the corresponding parameter spaces in Figure 5, it becomes clear that under the restriction of the given minimum film thickness, the maximum efficiency for $\mu = \mu_{ref}$ must be at $d =$ 200 nm, and $d = 328$ nm for $\mu = 100\mu_{ref}$, respectively. The model-based optimization approach with d_{true} can already identify the correct layer thickness after a few rounds of process optimization, regardless of the parameter space. Although the model-based optimization approach using the predicted layer thickness has the same information, it cannot predict the true layer thickness accurately enough. The result is a reduced peak height with an

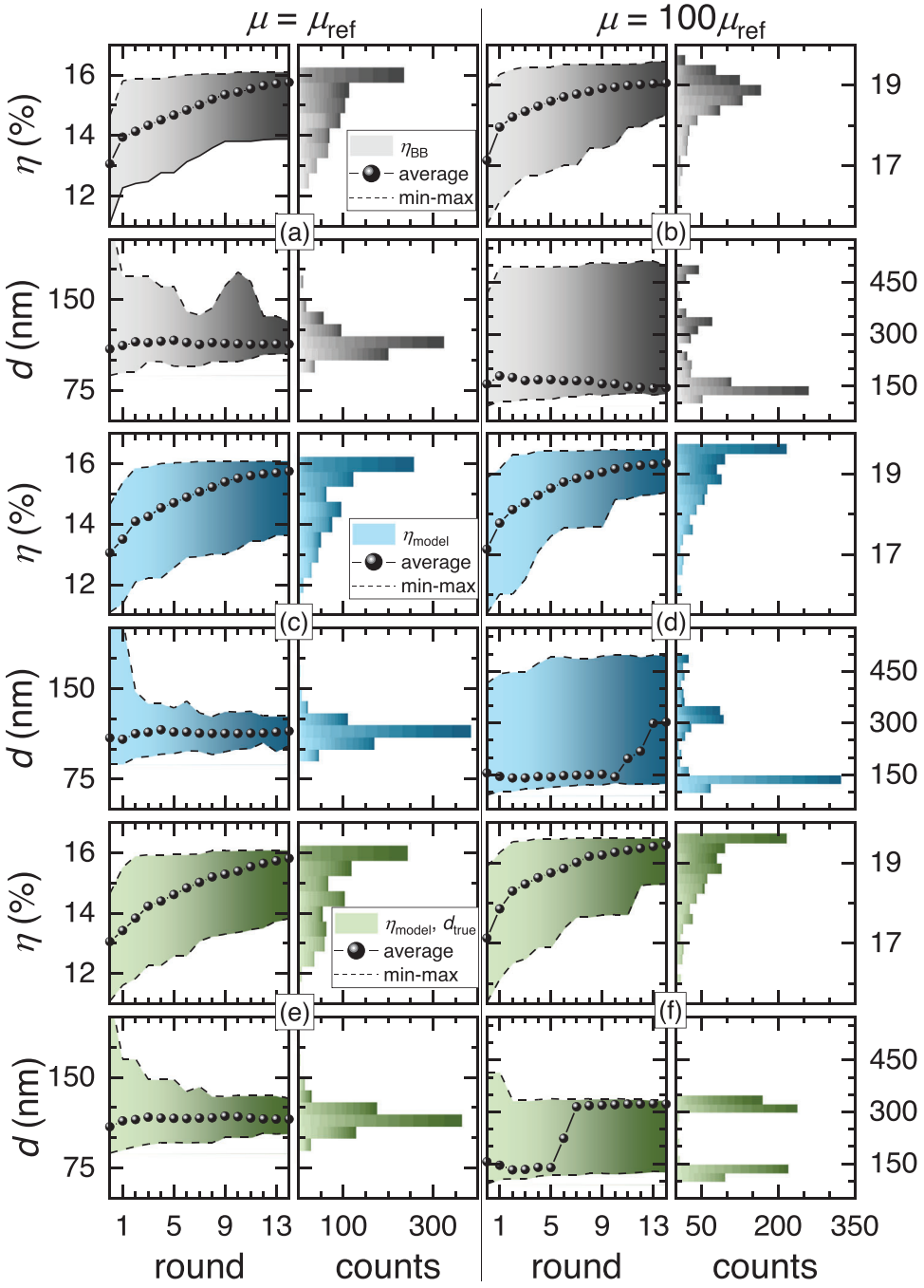

Figure 7. Comparison of the different process optimization approaches for $\mu = \mu_{ref}$ and $\mu = 100\mu_{ref}$. a) Purely black-box based process optimization for $\mu = \mu_{ref}$ based on 50 optimization runs with four associated figures: 1. mean efficiency and min-max range as a function of the actual optimizations round, 2. the histogram for the best efficiencies, 3. the associated median active layer thicknesses with min-max range as well as 4. the corresponding histogram. b) Analogous results for pure black-box optimization for $\mu = 100\mu_{ref}$. c–f) Analogous results for the other model-based optimization approaches.

increased peak width around the target layer thickness. In contrast to the two model-based approaches, both black-box approaches know nothing about the underlying physics, i.e., the thickness-dependent interference mechanisms. Information about the target layer thickness must be learned first; however, in the case of the black-box approach with a separate regression function for the layer thickness d_{fit}, this learning process is significantly faster owing to the explicit additional information about the layer thickness. However, this additional learning effort is a disadvantage compared to model-based approaches.

It should be noted that the results shown here represent an identifiable trend regarding the choice of parameter space. In general, it can be said that the difference between all optimization approaches is smaller for parameter spaces with a single strong

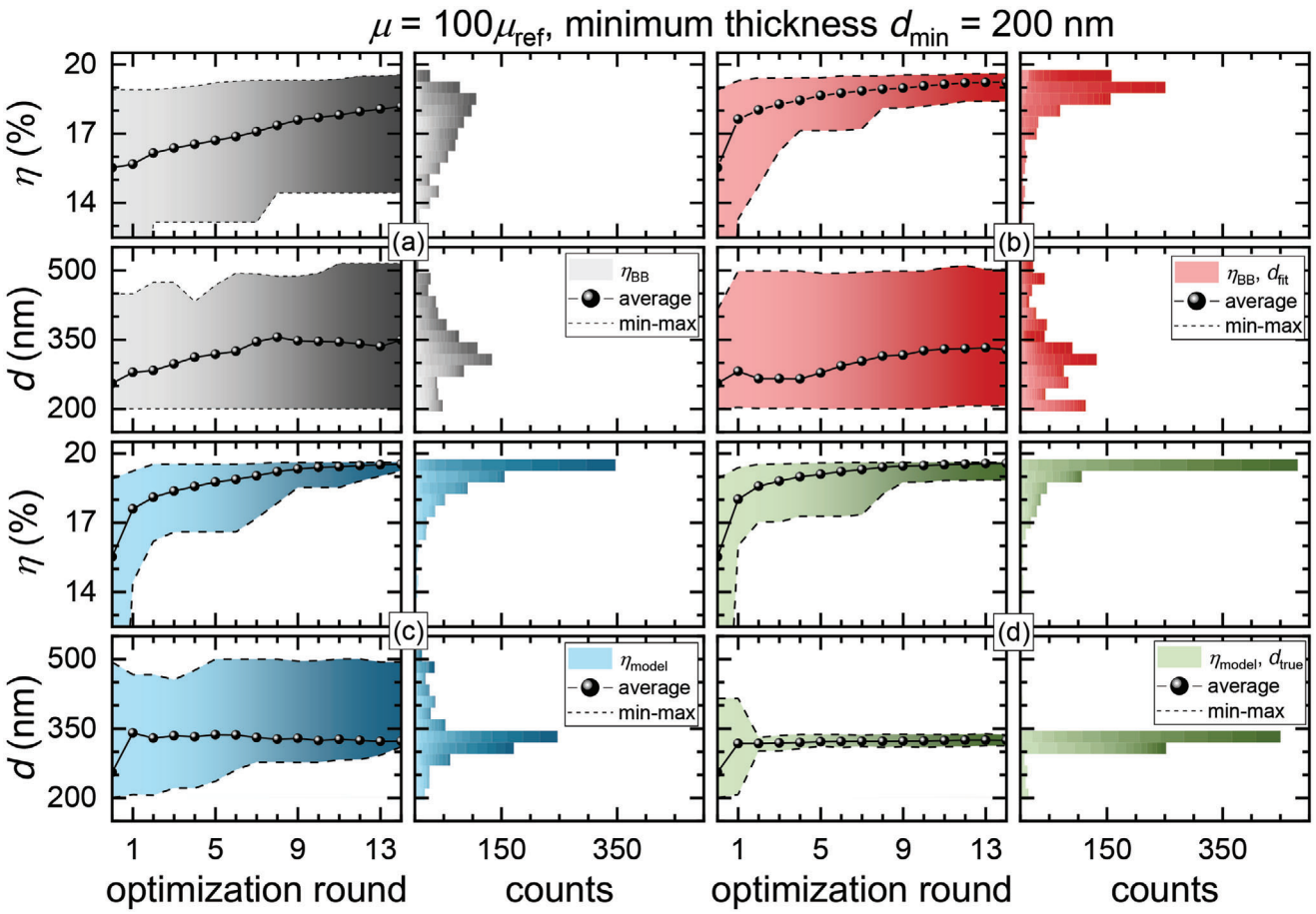

Figure 8. Comparison of the different process optimization approaches for $\mu = 100\mu_{ref}$ with an active layer restriction of $d > 200$ nm. a) Pure black-box process optimization based on 50 optimization runs with four associated figures: 1. mean efficiency and min-max range as a function of the actual optimizations round, 2. the histogram for the best efficiencies, 3. the associated median active layer thicknesses with min-max range as well as 4. the corresponding histogram. b) Analogous results for black-box optimization with fit function for layer thickness as well as c) the model-based approaches with d_{fit} and d) with d_{true} respectively.

global optimum. In the case of a second optimum, model-based approaches, especially those with adjustable layer thickness, have an advantage in identifying the optimal layer thickness and therefore in finding higher efficiencies.

We propose several possible explanations for our findings. We assume that the complexity of the individual regression functions describing the correlation between the process parameters and the regression parameter varies. The lower the complexity of a function, the smaller the amount of data required to describe it adequately. If we assume that the connection between $\mathbf{\Theta}_{pro}$ and $\mathbf{\Theta}_{mat}$ is less complex than that between $\mathbf{\Theta}_{pro}$ and η, we obtain a more precise model function for the former with the same amount of training data. Second, the higher accuracy of the model function can be attributed to the amount of information used from the measured JV curves. For the pure correlation between $\mathbf{\Theta}_{pro}$ and η, the information content is limited to a small part of the entire JV curve, that is, the maximum power point. However, by fitting the material parameters dependent on the entire shape of the JV curve (or by including additional characterization methods) significantly more information is used. Finally, most likely the strongest influence comes from the fact that the model-based approaches use the underlying physical domain knowledge when calculating the efficiency from each of its predicted material parameters and therefore the approaches "know" what effect material parameters will have on the resulting efficiency. **Figure 9** is intended to support the argumentation. The figure schematically illustrates two physical quantities that should make our argumentation more tangible. The first is the charge carrier collection efficiency η_{col}, and the second is the optical efficiency η_{opt}. The collection efficiency η_{col} describes how likely it is, that a generated charge carrier in the active layer finds its way to a contact. High charge carrier mobilities and low recombination coefficients lead to a high collection efficiency. Especially for high η_{col}, it is almost independent of the active layer thickness. The opposite is true for small μ and k. The optical efficiency η_{opt} mainly depends on light absorption. Local absorption maxima and minima are formed due to interferences and the shape is determined by the layer stack of the solar cell. Low values for η_{eh} reduce the efficiency for a given η_{opt}. Additionally, we added the final power conversion efficiency $\eta \propto \eta_{col} \bullet \eta_{opt}$ to

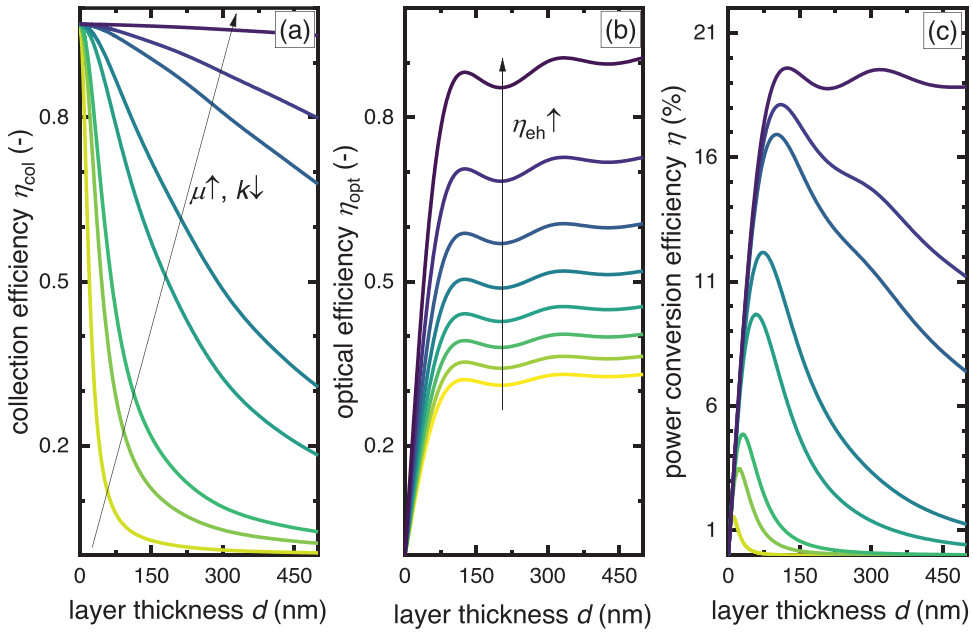

Figure 9. Schematic illustration for a) the charge carrier collection efficiency η_{col}, b) the optical efficiency η_{opt}, and c) the final power conversion efficiency for the solar cell η. The power conversion efficiency of the solar cell is proportional to the product of the collection efficiency and the optical efficiency: $\eta \propto \eta_{col} \bullet \eta_{opt}$. All four material parameters μ, k, η_{eh}, and d have a strong influence on the final (power conversion) efficiency of the solar cell. Additional knowledge about the more complex influence of the active layer thickness on η_{opt} such as the location of local optima can be particularly helpful during process optimization.

the figure. All efficiencies are shown as a function of the active layer thickness d. The presented correlations are now to be linked to the process parameters.

An obvious and very strong influence on the layer thickness comes from the spin speed.[58] The exact influence of the other process parameters on the active layer thickness is less well-known, but also much less pronounced. However, regardless of the influences in detail, all process parameters that affect the active layer thickness also have a strong correlation to η_{col} and η_{opt}. The significantly more complex influence on the latter can particularly be helpful for process optimization. The profound understanding of the correlation between layer thickness-dependent interference and the location of local maxima and minima significantly aids process optimization.

Process parameters, such as chemical mixing ratios or annealing conditions primarily determine the morphology of the active layer, and thereby they mostly determine μ, k, and η_{eh}.[59–63] Additional modeling of the morphological influences on the electronic properties of the solar cell is reasonable. This requires further measurements of the cell morphology in combination with appropriate models. Coarse-grained molecular dynamic methodologies might be a promising approach in this regard[59].

We assume that it is crucial to find usable models based on which the influence of decisive material parameters can be mapped during process optimization. Ideally, the corresponding physical models should be as simple as possible and as complex as necessary. The final composite model for the model-based process optimization would then be based exclusively on the crucial material parameters that have the strongest impact on the complexity of the parameter space. While the further device characterization of these key parameters would be particularly valuable, the less influential parameters can be adequately represented by a black-box. This combines the advantages of black-box optimization with model-based optimization.

5. Conclusion

Standard process optimization typically involves fabrication, measurement, evaluation, learning, and iteration. With the advent of optimization algorithms that leverage mathematical models in increasingly automated laboratories, the necessity for extensive measurements beyond the figure of merit has become increasingly questionable. To investigate this, we implemented a virtual laboratory based on our own experimental data from hundreds of organic solar cells. We emphasize again that this virtual laboratory is not intended to optimize a specific process as that process must be already optimized to create the benchmark function in the first place. Instead, the virtual laboratory serves as a less generic and more problem-specific benchmark function to compare different optimization approaches in the field of OPV. This benchmark function allows optimization algorithms to be compared very quickly, which also enables statistical evaluation. Additionally, the benchmark function is known. While with an unknown optimization problem, it always remains unclear whether the optimum found is a local or already the global optimum, with a known benchmark function the optimization algorithm can also be evaluated in absolute terms. In other words, the benchmark function solves the problems associated with long fabrication and measurement times.

However, the study is intended as food for thought to discuss the extent to which the understanding gained over decades in the field of (organic) photovoltaics can be used to accelerate process

optimization. The basis of the virtual laboratory considered here is a strong simplification; however, we assume that the main findings can be transferred to real applications.

The conclusions obtained from this virtual laboratory indicate that, under certain circumstances, it may be worthwhile to include knowledge of the physical background in process optimization. Two main examples are presented, where such additional knowledge can be beneficial for device optimization. The first example is the case where the material has significantly higher charge-carrier mobilities, where we imagine future improvements in material quality. These higher mobilities would lead to situations where further local or even global optima emerge at higher layer thicknesses and where the efficiency versus thickness landscape would be significantly more complicated than it is for low-mobility molecular semiconductors. While such a change in the parameter space for the black-box approach represents an increase in the complexity of the function to be optimized, the model-based approach has the information about the interferences and optics and can therefore predict how efficiency depends on thickness once it has relative rudimentary information on the electronic properties. The step from efficiency versus thickness to efficiency versus process parameters is still important and non-trivial but it is easier for the optimization algorithm than if nothing is known about the physics of light absorption.

Another example where higher active layer thicknesses become relevant are constraints imposed by technological considerations such as high-yield printing in a dust-containing atmosphere. We also show that it would be ideal to immediately know the thickness resulting from certain process parameters. Thus, in situ methods to quantify changes in thickness are likely to be helpful, especially for model-based optimization approaches.

Future research should explore how domain knowledge about other key parameters might be useful during process optimization in a comparable manner as is the case for the active layer thickness. In particular, the question of how additional device characterization regarding the morphology of the active layer can be valuable during model-based process optimization needs to be examined.

Supporting Information

Supporting Information is available from the Wiley Online Library or from the author.

Acknowledgements

The authors thank the Ministry of Economic Affairs, Industry, Climate Action and Energy of the State of North Rhine-Westphalia for funding via the ENFA ("Entwicklung effizienter ternärer NFA-basierter organischer Photovoltaik durch Machine-Learning Methoden") project.

Open access funding enabled and organized by Projekt DEAL.

Conflict of Interest

The authors declare no conflict of interest.

Data Availability Statement

The data that support the findings of this study are available from the corresponding author upon reasonable request.

Keywords

machine learning, organic photovoltaics, process optimization

Received: January 13, 2025
Revised: February 20, 2025
Published online: February 27, 2025

[1] J. M. Haffner-Schirmer, V. M. Le Corre, K. Forberich, H. J. Egelhaaf, T. Osterrieder, J. Wortmann, C. Liu, P. Weitz, T. Heumüller, A. J. Bornschlegl, J. Wachsmuth, A. Distler, M. Wagner, Z. Peng, L. Lüer, C. J. Brabec, *Adv. Energy Mater.* **2025**, 2403479.
[2] Z. Yao, Y. Lum, A. Johnston, L. M. Mejia-Mendoza, X. Zhou, Y. Wen, A. Aspuru-Guzik, E. H. Sargent, Z. W. Seh, *Nat. Rev. Mater.* **2022**, *8*, 202.
[3] Z.-W. Zhao, Y. Geng, A. Troisi, H. Ma, *Adv. Intell. Sys.* **2022**, *4*, 2100261.
[4] H. Wang, Y. Ji, Y. Li, *WIREs Comput. Mol. Sci.* **2019**, *10*, e1421.
[5] L. Ma, S. Zhang, J. Wang, Y. Xu, J. Hou, *Chem. Commun.* **2020**, *56*, 14337.
[6] T. Osterrieder, F. Schmitt, L. Lüer, J. Wagner, T. Heumüller, J. Hauch, C. J. Brabec, *Energy Environ. Sci.* **2023**, *16*, 3984.
[7] B. Cao, L. A. Adutwum, A. O. Oliynyk, E. J. Luber, B. C. Olsen, A. Mar, J. M. Buriak, *ACS Nano* **2018**, *12*, 7434.
[8] W. Yang, W. Wang, Y. Wang, R. Sun, J. Guo, H. Li, M. Shi, J. Guo, Y. Wu, T. Wang, G. Lu, C. J. Brabec, Y. Li, J. Min, *Joule* **2021**, *5*, 1209.
[9] H. Chen, Y. Huang, R. Zhang, H. Mou, J. Ding, J. Zhou, Z. Wang, H. Li, W. Chen, J. Zhu, Q. Cheng, H. Gu, X. Wu, T. Zhang, Y. Wang, H. Zhu, Z. Xie, F. Gao, Y. Li, Y. Li, *Nat. Mater.* **2025**, 1.
[10] Y. Jiang, S. Sun, R. Xu, F. Liu, X. Miao, G. Ran, K. Liu, Y. Yi, W. Zhang, X. Zhu, *Nat. Energy* **2024**, *9*, 975.
[11] X. Liao, M. Liu, H. Pei, P. Zhu, X. Xia, Z. Chen, Y. Zhang, Z. Wu, Y. Cui, G. Xu, M. Gao, L. Ye, R. Ma, T. Liu, X. Lu, H. Zhu, Y. Chen, *Angew. Chem., Int. Ed.* **2024**, *63*, 202318595.
[12] J. Wang, Z. Zheng, P. Bi, Z. Chen, Y. Wang, X. Liu, S. Zhang, X. Hao, M. Zhang, Y. Li, J. Hou, *Natl. Sci. Rev.* **2023**, *10*, nwad085.
[13] Y. Cui, Y. Xu, H. Yao, P. Bi, L. Hong, J. Zhang, Y. Zu, T. Zhang, J. Qin, J. Ren, Z. Chen, C. He, X. Hao, Z. Wei, J. Hou, *Adv. Mater.* **2021**, *33*, 2102420.
[14] C. He, Y. Pan, Y. Ouyang, Q. Shen, Y. Gao, K. Yan, J. Fang, Y. Chen, C.-Q. Ma, J. Min, C. Zhang, L. Zuo, H. Chen, *Energy Environ. Sci.* **2022**, *15*, 2537.
[15] S. Guan, Y. Li, C. Xu, N. Yin, C. Xu, C. Wang, M. Wang, Y. Xu, Q. Chen, D. Wang, L. Zuo, H. Chen, *Adv. Mater.* **2024**, *36*, 2400342.
[16] T. H. Kim, N. W. Park, M. A. Saeed, S. Y. Jeong, H. Y. Woo, J. Park, J. W. Shim, *Nano Energy* **2023**, *112*, 108429.
[17] S. Lai, Y. Cui, Z. Chen, X. Xia, P. Zhu, S. Shan, L. Hu, X. Lu, H. Zhu, X. Liao, Y. Chen, *Adv. Mater.* **2024**, *36*, 2313105.
[18] Y. Cui, H.-F. Yao, Y. Xu, P.-Q. Bi, J.-Q. Zhang, T. Zhang, L. Hong, Z.-H. Chen, Z.-X. Wei, X.-T. Hao, J.-H. Hou, *Chin. J. Polym. Sci.* **2022**, *40*, 979.
[19] A. Distler, C. J. Brabec, H.-J. Egelhaaf, *Prog. Photovoltaics* **2020**, *29*, 24.
[20] R. Po, A. Bernardi, A. Calabrese, C. Carbonera, G. Corso, A. Pellegrino, *Energy Environ. Sci.* **2014**, *7*, 925.
[21] G. Wang, M. A. Adil, J. Zhang, Z. Wei, *Adv. Mater.* **2018**, *31*, 1805089.
[22] S. Yoon, S. Park, S. H. Park, S. Nah, S. Lee, J.-W. Lee, H. Ahn, H. Yu, E.-Y. Shin, B. J. Kim, B. K. Min, J. H. Noh, H. J. Son, *Joule* **2022**, *6*, 2406.
[23] X. Yang, Y. Shao, S. Wang, M. Chen, B. Xiao, R. Sun, J. Min, *Adv. Mater.* **2023**, 2307863.

[24] A. Armin, W. Li, O. J. Sandberg, Z. Xiao, L. Ding, J. Nelson, D. Neher, K. Vandewal, S. Shoaee, T. Wang, H. Ade, T. Heumüller, C. Brabec, P. Meredith, *Adv. Energy Mater.* **2021**, *11*, 2003570.
[25] M. Kim, S. U. Ryu, S. A. Park, Y.-J. Pu, T. Park, *Chem. Sci.* **2021**, *12*, 14004.
[26] P. Cheng, G. Li, X. Zhan, Y. Yang, *Nat. Photonics* **2018**, *12*, 131.
[27] J. Gao, J. Wang, C. Xu, Z. Hu, X. Ma, X. Zhang, L. Niu, J. Zhang, F. Zhang, *Sol. RRL* **2020**, *4*, 2000364.
[28] E. Destouesse, M. Top, J. Lamminaho, H.-G. Rubahn, J. Fahlteich, M. Madsen, *Flexible Printed Electron* **2019**, *4*, 045004.
[29] R. Søndergaard, M. Hösel, D. Angmo, T. T. Larsen-Olsen, F. C. Krebs, *Mater. Today* **2012**, *15*, 36.
[30] D. Weichert, P. Link, A. Stoll, S. Rüping, S. Ihlenfeldt, S. Wrobel, *Int. J. Adv. Manuf. Technol.* **2019**, *104*, 1889.
[31] R. J. Hickman, M. Aldeghi, F. Häse, A. Aspuru-Guzik, *Digital Discovery* **2022**, *1*, 732.
[32] P. I. Frazier, *Bayesian Optimization, INFORMS Tutorials in Oper. Res.* **2018**, 255.
[33] X. Du, L. Lüer, T. Heumueller, J. Wagner, C. Berger, T. Osterrieder, J. Wortmann, S. Langner, U. Vongsaysy, M. Bertrand, N. Li, T. Stubhan, J. Hauch, C. J. Brabec, *Joule* **2021**, *5*, 495.
[34] X. Rodríguez-Martínez, E. Pascual-San-José, M. Campoy-Quiles, *Energy Environ. Sci.* **2021**, *14*, 3301.
[35] J. Zhang, J. A. Hauch, C. J. Brabec, *Acc. Chem. Res.* **2024**, *57*, 1434.
[36] G. Tom, S. P. Schmid, S. G. Baird, Y. Cao, K. Darvish, H. Hao, S. Lo, S. Pablo-García, E. M. Rajaonson, M. Skreta, N. Yoshikawa, S. Corapi, G. D. Akkoc, F. Strieth-Kalthoff, M. Seifrid, A. Aspuru-Guzik, *Chem. Rev.* **2024**, *124*, 9633.
[37] A. Kristiadi, F. Strieth-Kalthoff, S. G. Subramanian, V. Fortuin, P. Poupart, G. Pleiss, arXiv:2406.06459 **2024**.
[38] Z. Ren, F. Oviedo, M. Thway, S. I. P. Tian, Y. Wang, H. Xue, J. D. Perea, M. Layurova, T. Heumueller, E. Birgersson, A. G. Aberle, C. J. Brabec, R. Stangl, Q. Li, S. Sun, F. Lin, I. M. Peters, T. Buonassisi, *npj Comput. Mater.* **2020**, *6*, 9.
[39] F. Häse, M. Aldeghi, R. J. Hickman, L. M. Roch, A. Aspuru-Guzik, *Appl. Phys. Rev.* **2021**, *8*, 031406.
[40] H. J. A. F. Tulleken, *Automatica* **1993**, *29*, 285.
[41] R. Astudillo, P. I. Frazier, presented at 2021 Winter Sim. Conf. (WSC), IEEE, Phoenix, AZ, USA **2021**.
[42] R. Astudillo, P. I. Frazier, *Int. Conf. Mach. Learn* **2019**, *97*, 354.
[43] M. Jamil, X. S. Yang, *Int. J. Math. Modell. Numer. Optim.* **2013**, *4*, 150.
[44] B. Y. Qu, J. J. Liang, Z. Y. Wang, Q. Chen, P. N. Suganthan, *Swarm Evol. Comput.* **2016**, *26*, 23.
[45] K. Hussain, M. N. Mohd Salleh, S. Cheng, R. Naseem, *JOIV Int. J. Inf. Visualization* **2017**, *1*, 218.
[46] L. Hong, H. Yao, Z. Wu, Y. Cui, T. Zhang, Y. Xu, R. Yu, Q. Liao, B. Gao, K. Xian, H. Y. Woo, Z. Ge, J. Hou, *Adv. Mater.* **2019**, *31*, 1903441.
[47] L. Meng, Y. Zhang, X. Wan, C. Li, X. Zhang, Y. Wang, X. Ke, Z. Xiao, L. Ding, R. Xia, H.-L. Yip, Y. Cao, Y. Chen, *Sci* **2018**, *361*, 1094.
[48] G. F. Burkhard, E. T. Hoke, M. D. McGehee, *Adv. Mater.* **2010**, *22*, 3293.
[49] R. E. I. Schropp, M. Zeman, *Electrical Device Modeling*, Springer, Boston **1998**.
[50] B. Das, *Defect tolerant device geometries for lead-halide perovskite solar cells*, Rheinisch-Westfälische Technische Hochschule Aachen, **Aachen 2022**.
[51] P. Hartnagel, *Simulation and Characterization of Energetic Disorder and Recombination in Organic Solar Cells*, Universität Duisburg-Essen, **Duisburg 2024**.
[52] R. E. Brandt, R. C. Kurchin, V. Steinmann, D. Kitchaev, C. Roat, S. Levcenco, G. Ceder, T. Unold, T. Buonassisi, *Joule* **2017**, *1*, 843.
[53] M. Hußner, R. A. Pacalaj, G. Olaf Müller-Dieckert, C. Liu, Z. Zhou, N. Majeed, S. Greedy, I. Ramirez, N. Li, S. M. Hosseini, C. Uhrich, C. J. Brabec, J. R. Durrant, C. Deibel, R. C. I. MacKenzie, *Adv. Energy Mater.* **2023**, *14*, 2303000.
[54] S. Bhatti, H. U. Manzoor, B. Michel, R. S. Bonilla, R. Abrams, A. Zoha, S. Hussain, R. Ghannam, *Adv. Energy Sustainability Res.* **2023**, *4*, 2300004.
[55] Q. Song, Y. Bai, Q. Chen, *J. Phys. Chem. Lett.* **2022**, *13*, 10741.
[56] V. Beiranvand, W. Hare, Y. Lucet, *Optim. Eng.* **2017**, *18*, 815.
[57] N. G. An, J. Y. Kim, D. Vak, *Energy Environ. Sci.* **2021**, *14*, 3438.
[58] P. C. Sukanek, *J. Electrochem. Soc.* **1991**, *138*, 1712.
[59] T. Wang, G. Kupgan, J.-L. Brédas, *Trends Chem* **2020**, *2*, 535.
[60] K. Vandewal, *Annu. Rev. Phys. Chem.* **2016**, *67*, 113.
[61] J. Nelson, J. J. Kwiatkowski, J. Kirkpatrick, J. M. Frost, *Acc. Chem. Res.* **2009**, *42*, 1768.
[62] S. Foster, F. Deledalle, A. Mitani, T. Kimura, K.-B. Kim, T. Okachi, T. Kirchartz, J. Oguma, K. Miyake, J. R. Durrant, S. Doi, J. Nelson, *Adv. Energy Mater.* **2014**, *4*, 1400311.
[63] S. A. Mollinger, K. Vandewal, A. Salleo, *Adv. Energy Mater.* **2015**, *5*, 1501335.